Cnossen, I., Förster, M. (2016): North-South asymmetries in the polar thermosphere-ionosphere system: Solar cycle and seasonal influences. - *Journal of Geophysical Research*, *121*, 1, pp. 612—627.

DOI: http://doi.org/10.1002/2015JA021750

AGU PUBLICATIONS

JGR

Journal of Geophysical Research: Space Physics

RESEARCH ARTICLE
10.1002/2015JA021750

Key Points:
- North-south asymmetries in high-latitude ion drift speed depend on season and solar activity
- High-latitude neutral wind speeds are always larger in summer, regardless of solar activity
- The CMIT model can explain the ion drift results but does not capture the neutral wind behavior

Correspondence to:
I. Cnossen,
inos@bas.ac.uk

Citation:
Cnossen, I., and M. Förster (2016), North-south asymmetries in the polar thermosphere-ionosphere system: Solar cycle and seasonal influences, *J. Geophys. Res. Space Physics*, *121*, 612–627, doi:10.1002/2015JA021750.

Received 31 JUL 2015
Accepted 7 DEC 2015
Accepted article online 12 DEC 2015
Published online 16 JAN 2016

North-south asymmetries in the polar thermosphere-ionosphere system: Solar cycle and seasonal influences

Ingrid Cnossen[1] and Matthias Förster[2]

[1]British Antarctic Survey, Cambridge, UK, [2]GFZ German Research Centre for Geosciences, Potsdam, Germany

Abstract Previous studies have revealed that ion drift and neutral wind speeds at ~400 km in the polar cap (>80° magnetic latitude) are on average larger in the Northern Hemisphere (NH) than in the Southern Hemisphere, which is at least partly due to asymmetry in the geomagnetic field. Here we investigate for the first time how these asymmetries depend on season and on solar/geomagnetic activity levels. Ion drift measurements from the Cluster mission show little seasonal dependence in their north-south asymmetry when all data (February 2001–December 2013) are used, but the asymmetry disappears around June solstice for high solar activity and around December solstice for low solar activity. Neutral wind speeds in the polar cap obtained from the Challenging Minisatellite Payload spacecraft (January 2002–December 2008) are always larger in the summer hemisphere, regardless of solar activity, but the high-latitude neutral wind vortices at dawn and dusk tend to be stronger in the NH, except around December solstice, in particular, when solar activity is low. Simulations with the Coupled Magnetosphere-Ionosphere-Thermosphere (CMIT) more or less capture the behavior of the ion drift speeds, which can be explained as a superposition of seasonal and geomagnetic field effects, with the former being stronger for higher solar activity. The behavior of the neutral wind speed and vorticity is not accurately captured by the model. This is probably due to an incorrect seasonal cycle in plasma density around ~400 km in CMIT, which affects the ion drag force. This must be addressed in future work.

1. Introduction

Disturbances in the solar wind and the interplanetary magnetic field (IMF) affect the Earth's high-latitude thermosphere and ionosphere via coupling with the magnetosphere. To first order, one might expect this coupling to occur symmetrically between the two hemispheres. Indeed, it is often assumed that the Northern Hemisphere (NH) and Southern Hemisphere (SH) are mirror images of each other, although with the understanding that (1) seasonal effects can cause asymmetries, particularly at solstice and (2) the B_y component of the IMF has the opposite effect in the NH and SH [e.g., *Pettigrew et al.*, 2010]. However, statistical studies by *Förster et al.* [2007, 2008, 2011] have shown that even when those effects are taken into account, there are systematic differences between the high-latitude NH and SH upper atmosphere. Ion drifts measured with the Electron Drift Instrument (EDI) on board the Cluster satellite fleet are stronger in the NH than SH. Neutral winds measured with the accelerometer on board the Challenging Minisatellite Payload (CHAMP) spacecraft also have larger speeds in the NH than in the SH, and similarly, the neutral wind vorticity is higher in the NH. In contrast, the spatial variance of the neutral wind patterns is larger in the SH than in the NH. These north-south asymmetries can be thought of as a large-scale, low-order modulation of the Earth's upper atmosphere response to space weather. It is important to understand this modulation better because of the increasing amount of satellite-based technology operating within the upper atmosphere.

Simulations with the Coupled Magnetosphere-Ionosphere-Thermosphere (CMIT) model have demonstrated that north-south differences in the polar upper atmosphere can be explained at least to some extent by asymmetries in the Earth's magnetic field, both in magnetic flux density and in the offset between the geographic and invariant magnetic poles in the two hemispheres [*Förster and Cnossen*, 2013]. First, the magnetic flux density (**B**) in the NH polar region is smaller than in the SH polar region. Idealized studies by *Cnossen et al.* [2011, 2012a] showed that a weaker magnetic field strength results in a weaker high-latitude electric field (**E**), but the $\mathbf{E}\times\mathbf{B}$ drift magnitude, which scales as E/B, is still larger for a weaker magnetic field. This can explain the larger $\mathbf{E}\times\mathbf{B}$ drift speeds in the NH, while simultaneously fitting with observational evidence indicating that the cross-polar cap potential (CPCP), a good measure of the high-latitude electric field strength, is on average

~5–10% larger in the SH [*Papitashvili and Rich*, 2002; *Pettigrew et al.*, 2010; *Förster and Haaland*, 2015]. Second, the offset between the invariant magnetic pole and the geographic pole is smaller in the NH than the SH, which can be interpreted as a smaller tilt angle in the NH. A smaller tilt angle generally gives a larger CPCP, which will result in larger $\mathbf{E} \times \mathbf{B}$ drifts [*Cnossen and Richmond*, 2012]. However, this effect should give a larger CPCP in the NH, which is not consistent with the observations by *Papitashvili and Rich* [2002], *Pettigrew et al.* [2010], and *Förster and Haaland* [2015]. From this we can conclude that the north-south asymmetry in the offset between the invariant magnetic pole and geographic pole is probably less important than the north-south asymmetry in magnetic flux density for creating the observed asymmetries in $\mathbf{E} \times \mathbf{B}$ drift speeds. On the other hand, the smaller offset in the NH could explain why the spatial variance in neutral winds is smaller in the NH; forces acting on the neutral wind in a geographic reference frame, such as the pressure gradient and Coriolis force, will be more closely aligned with forces acting in a magnetic reference frame, such as the ion drag force. In contrast, when the offset between the invariant magnetic pole and the geographic pole is larger, as in the SH, these forces will act in somewhat different directions, resulting in greater variance.

While *Förster and Cnossen* [2013] could explain several of the key features of observed north-south asymmetries in the high-latitude upper atmosphere, there are still a number of remaining questions. Their simulations were done for the March equinox season of the year 2008, during solar minimum conditions, while the observational results on north-south asymmetries that they compared their model results with were based on data from all seasons and also included higher solar and geomagnetic activity levels. Both the season and the solar and geomagnetic activity levels are likely to interact with north-south asymmetries produced by the Earth's magnetic field, for instance, by changing the ionospheric conductivity in the polar regions. This has consequences for magnetosphere-ionosphere coupling processes, as well as ion-neutral coupling within the upper atmosphere. Here we will therefore explore in further detail how seasonal and solar/geomagnetic activity variations affect north-south asymmetries in the high-latitude upper atmosphere. We will use a combination of observational data from Cluster/EDI (plasma drift) and CHAMP (neutral winds) and simulations with the CMIT model. Further information about the observations, the model, the setup of the simulations, and the analysis procedures is provided in section 2. We present and discuss results on ion drifts, neutral winds, and neutral wind vorticity in sections 3, 4, and 5, respectively. In section 6 we summarize the key findings and provide an outlook to future work needed to resolve outstanding questions.

2. Methods

2.1. Observations

We use measurements of the ion drifts made by the EDI instrument on board the Cluster mission [*Escoubet et al.*, 1997] made between February 2001 and December 2013, comprising a full solar cycle. The electric field measurements at Cluster altitudes were mapped to an altitude of ~400 km in the upper atmosphere of both polar regions along geomagnetic field lines, assuming these can be treated as equipotential lines and assuming steady state conditions. The mapping is performed with the Tsyganenko T01 magnetic field model [*Tsyganenko*, 2002a, 2002b], which takes the solar wind and IMF conditions into account. More details about the method to obtain ionospheric projections of the magnetospheric plasma drifts are described by *Haaland et al.* [2007] and by *Förster and Haaland* [2015] in their latest update on EDI observations.

The neutral wind measurements come from a newly developed accelerometer on board CHAMP [*Reigber et al.*, 2002]. Data were obtained from 2002 to 2008, when CHAMP orbited the Earth in a circular, near-polar orbit at ~350–400 km. We use the data that were reanalyzed and recalibrated by the European Space Agency as described by *Doornbos et al.* [2010]. The triaxial accelerometer on board CHAMP allows estimation of only one component of the horizontal neutral wind along its orbital path, which is deduced from accelerations perpendicular to the bulk flow velocity. This wind component is close to the horizontal cross-track direction of the spacecraft. Near-polar full vector reconstructions of the horizontal neutral wind pattern can therefore be obtained only in a statistical approach over certain time intervals as described by *Förster et al.* [2008]. Ideally, one needs a period of ~131 days, which corresponds to the precession interval of CHAMP through all local times. Neutral wind vorticity patterns can be obtained as derivatives of the circumpolar neutral wind pattern of both the NH and the SH [see also *Förster et al.*, 2011].

2.2. Model Description

We use the Coupled Magnetosphere-Ionosphere-Thermosphere (CMIT) model [*Wiltberger et al.*, 2004; *Wang et al.*, 2004, 2008] to examine north-south differences in the high-latitude upper atmosphere.

CMIT couples the Lyon-Fedder-Mobarry (LFM) global magnetospheric code [*Lyon et al.*, 2004] with the Thermosphere-Ionosphere-Electrodynamics general circulation model (TIE-GCM) [*Roble et al.*, 1988; *Richmond et al.*, 1992] through the MIX coupler module [*Merkin and Lyon*, 2010].

The LFM component of the model solves the ideal magnetohydrodynamic (MHD) equations to simulate the interaction between the solar wind and the magnetosphere and calculates the full MHD state vector (plasma density, pressure, velocity, and magnetic field). It requires the solar wind MHD state vector on its outer boundary as input and uses an empirical parameterization [*Wiltberger et al.*, 2009] to calculate the energy flux of precipitating electrons. On its inner boundary it requires the ionospheric conductance to calculate the electric potential, which is passed in from the TIE-GCM part of the code through the MIX module.

The TIE-GCM is a time-dependent, three-dimensional model that solves the fully coupled, nonlinear, hydrodynamic, thermodynamic, and continuity equations of the thermospheric neutral gas self-consistently with the ion continuity equations. At high latitudes it requires the auroral particle precipitation and electric field imposed from the magnetosphere, which it receives from the MIX component of the code. The solar activity level is specified through both a daily $F_{10.7}$ value and an 81 day mean $F_{10.7}$ value. At the lower boundary (~97 km altitude), tidal forcing can be provided by the global scale wave model (GSWM). In our simulations we used the GSWM migrating diurnal and semidiurnal tides [*Hagan and Forbes*, 2002, 2003]. The TIE-GCM component of the model was run with a $5° \times 5°$ global grid.

The coupling of the LFM and TIE-GCM in CMIT enables the calculation of the global ionospheric electric field, which includes both the imposed high-latitude electric field from the magnetosphere and the dynamo electric fields generated by thermospheric winds. This makes CMIT a two-way coupled model, in which the magnetosphere is able to influence the ionosphere-thermosphere system and vice versa.

2.3. Simulation Setup

The CMIT model cannot reasonably be run for full years; this would require too much computing resource. Therefore, we use a series of simulations with CMIT for different seasons and different background solar and geomagnetic activity levels. These simulations are summarized in Table 1 with identifiers that will be used in the remainder of the text for easy reference. All start and end dates are at 0 UT. Average $F_{10.7}$ and *Kp* index levels for each simulation interval are given as an indication of the solar and geomagnetic activity levels.

The first three simulations are all run for periods of ~3 weeks in 2002–2003, when solar and geomagnetic activity levels were medium high, for three different seasons: December solstice (dsol-hh), June solstice (jsol-mh), and March equinox (meq-mh). We investigate the influence of different seasons on north-south asymmetries mainly by comparing these simulations with each other.

The following two simulations are run for the full month of January in 2012 (dsol-mm) and 2010 (dsol-ll), which represent medium and low solar and geomagnetic activity levels, respectively. Comparing these simulations to the dsol-hh simulation will give insight in the dependence of north-south asymmetries on the background solar and geomagnetic activity level for December solstice. Simulation jsol-lm offers an opportunity to investigate the influences of background solar and geomagnetic activity levels for June solstice, as for this interval (June 2010) the solar activity level was very low, comparable to dsol-ll, but geomagnetic activity was higher, comparable to dsol-mm.

We further test the influence of changes in solar activity level separately with the final two simulations, which simulate the same intervals as dsol-hh and jsol-mh, respectively, but with the $F_{10.7}$ levels artificially reduced to 80 solar flux units (sfu).

2.4. Analysis Procedures

All data were transformed from geographic to altitude-adjusted corrected geomagnetic coordinates [*Baker and Wing*, 1989]. Only data poleward of 80° magnetic latitude were selected to isolate the central polar cap regions in both hemispheres. Neutral wind speed measurements were initially collected into equal-area squared bins of 2° width in latitude, with the length in the longitudinal direction chosen such to form a square, giving 78 bins for each polar cap region. Full neutral wind vectors were determined from all the one-component measurements within a bin over a certain time interval. To avoid biases due to inhomogeneous local time coverage, the optimal time interval to use is 131 days, as this corresponds to a full local time

Table 1. List of Simulations With Identifiers for Reference[a]

Identifier	Start Date	End Date	$F_{10.7}$ ($F_{10.7}$a)	*Kp*
dsol-hh	17 Dec 2002	7 Jan 2003	144 (146)	2.5
jsol-mh	20 Jun 2003	10 Jul 2003	130 (131)	2.9
meq-mh	20 Mar 2003	9 Apr 2003	128 (126)	3.2
dsol-mm	1 Jan 2012	1 Feb 2012	129 (124)	1.5
dsol-ll	1 Jan 2010	1 Feb 2010	78 (79)	0.7
jsol-lm	1 Jun 2010	1 Jul 2010	75 (77)	1.5
dsol-lh	17 Dec 2002	7 Jan 2003	80 (80)	2.5
jsol-lh	20 Jun 2003	10 Jul 2003	80 (80)	2.9

[a]The two $F_{10.7}$ values are the daily and 81 day average ($F_{10.7}$a) values in sfu, averaged over each simulation interval. Both are used as input to CMIT, though in the simulations they vary over time according to observations (except for dsol-lh and jsol-lh). The *Kp* index is not used as input to the model, but the average over each simulation interval is indicated to give an impression of the geomagnetic activity level.

scan by CHAMP. However, we are looking at very high latitudes, where local time biases will be small. To resolve seasonal variations better, we therefore used a binning window of 91 days here. Note that this combines measurements from different years for the same day of year (DOY) range to provide enough measurements in each bin. Seasonal variations were obtained by moving the 91 day window by 10 days at a time, so that we have 37 overlapping windows covering the whole year. The values for all spatial bins in the polar cap region (78 per hemisphere) were averaged to give a mean neutral wind for each of the 37 time windows. We also calculated the 95% confidence interval on this mean value, taking each of the 78 bin values as an independent data point. For the ion drifts, each data point is a full vector measurement, so that a two-step averaging procedure as for the neutral winds is not needed. We averaged all the ion drift measurements within the polar cap region and within a given 91 day window (same as for the neutral windows) to give a mean ion drift speed. The 95% confidence interval on the mean ion drift speed was calculated considering each individual measurement as an independent data point. The entire analysis was done both using the full data sets and separately for high (2002–2003) and low (2005–2007) solar activity years. To test the robustness of the results, we also performed the analysis with window lengths of 71 and 131 days, but this gave similar results, and we therefore only show results for the 91 day window length.

The neutral wind vorticity was calculated from all of the neutral wind data, i.e., not restricted anymore to magnetic latitudes >80°, but still focusing on the polar regions (> ~60° magnetic latitude) to capture the foci of the two vortices at high latitudes [see, e.g., *Förster et al.*, 2011]. The vorticity values we show correspond to the curl of the velocity field, given in units of megacycles per second. Considering that it is primarily the ion drag force that drives vortex structures in the high-latitude neutral wind, this can be considered as the part of the neutral wind field that relates most closely to forcing from the solar wind and magnetosphere. Vorticity maxima and minima were calculated to characterize the strength of the vortices. All of this analysis was done in the same way for the observations and the model results and in the same way as was done by *Förster and Cnossen* [2013]. For the neutral wind vorticity maxima and minima, the local time coverage of CHAMP matters more, because this is including data from lower latitudes. We therefore use the 131 day running averages to show the seasonal variation in these quantities, although again similar results (but somewhat less smooth) were obtained with a 91 day averaging window. It is not possible to calculate 95% confidence intervals on the vorticity maxima and minima, as we only have a single value for these quantities in each 131 day window.

The model data do not suffer from limited local time coverage but do not provide data for a full year, so that we cannot avoid using a different method for analyzing the seasonal variations in the model data. Each simulation was done for a specific season, and therefore, the model data were time averaged over each simulation interval for comparison with the observations. The corresponding standard deviations were used to calculate the 95% confidence intervals on the time-averaged values to establish the statistical significance of any differences between simulations.

3. Ion Drift Speed

Figure 1 shows the average ion drift speed in the polar cap (>80° magnetic latitude) based on Cluster/EDI measurements as a function of day of year in both hemispheres. When all data from 2001 to 2013 are used,

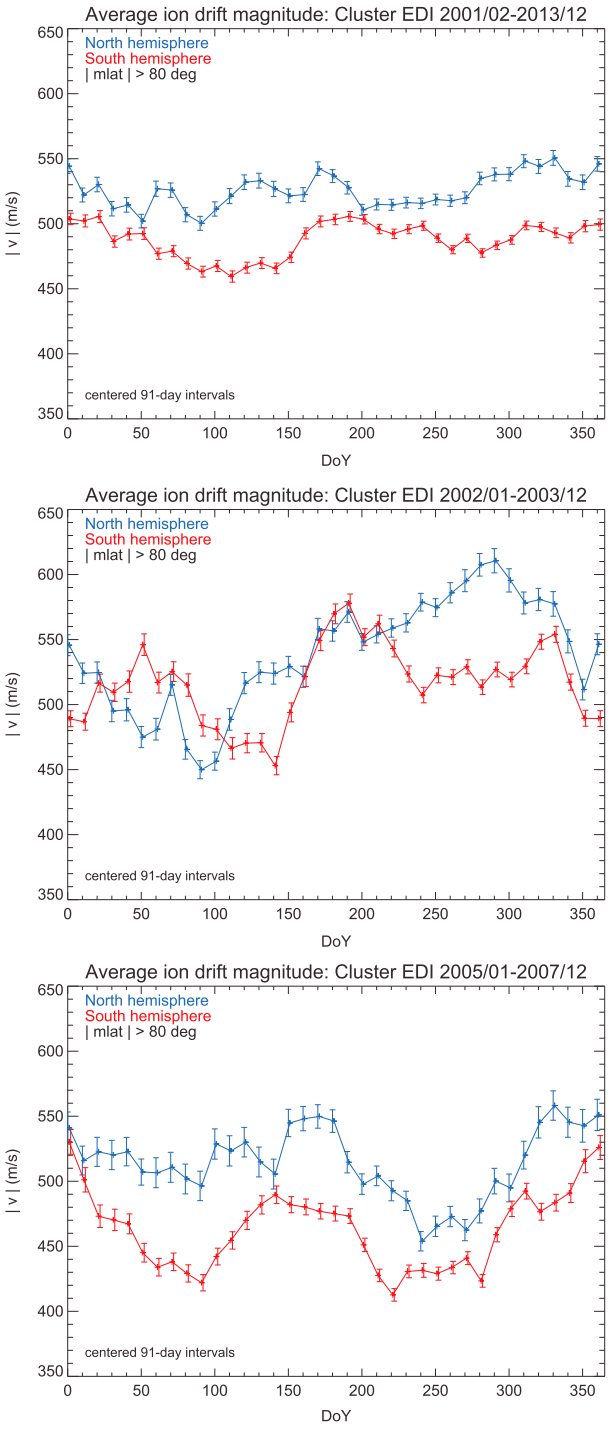

Figure 1. 91 day running averages of the mean ion drift speed in the polar cap (>80° magnetic latitude) for the NH (blue) and SH (red) based on EDI Cluster data from (top) February 2001 to December 2013 and separately for high solar activity years ((middle) 2002–2003) and low solar activity years ((bottom) 2005–2007). Error bars represent the 95% confidence intervals on the means.

we see relative little variation in the north-south difference with season: ion drift speeds are consistently larger, by ~10–50 m/s, in the NH than in the SH. There is also little seasonal variation within each hemisphere. However, when we perform the analysis separately for years of high solar activity (2001–2003) and low solar activity (2005–2007), there are some seasonal differences. For the high solar activity case, we find that the north-south asymmetry in ion drift speed more or less disappears around June solstice, while this happens around December solstice for the low solar activity case. Also, for the low solar activity years there appears to be a semiannual variation in ion drift speeds, in particular, in the SH, with maxima near the solstices and minima near the equinoxes. For high solar activity years there are some seasonal variations, but they do not follow a clear pattern. This could be due to influences of geomagnetic disturbances, which are on average more frequent and intense around solar maximum. Because geomagnetic activity peaks during equinox periods, this could level out the type of semiannual variation that was found for low solar activity, or in some cases it can even dominate the seasonal variations. For instance, the large ion drift speeds in the NH in October and November for the high solar activity case are probably associated with the Halloween storms in 2003.

We now turn to the CMIT model results. As an example, Figure 2 shows time series of the ion drift speed in the polar cap regions of both hemispheres for the first three simulations listed in Table 1. All of these are for intervals in 2002–2003 (high solar activity), but for different seasons. In agreement with the observations for high solar activity years, the north-south difference is very small (~10 m/s on average, not significant) for June solstice, and clearly more pronounced (~90 m/s on average) for March equinox and December solstice.

To summarize the results for all simulations listed in Table 1, we have calculated the average of the high-latitude ion drift speeds over each simulation interval for the NH and SH (i.e., averages of time series such as shown in Figure 2) and the 95% confidence interval on those averages. This information is presented in

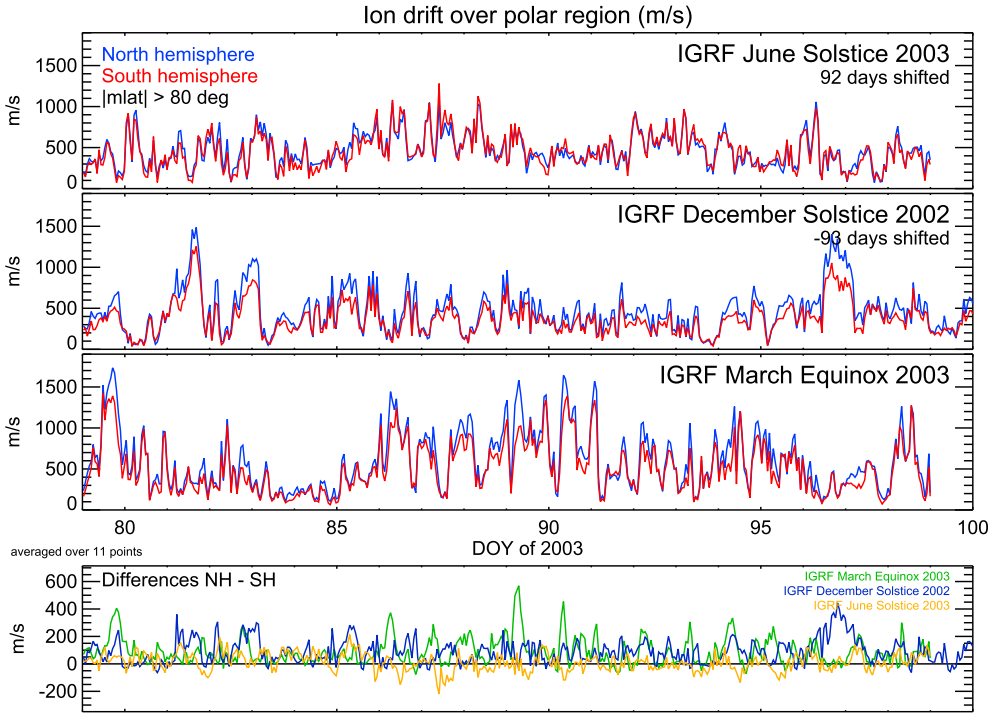

Figure 2. Mean ion drift speed in the polar cap (>80° magnetic latitude) for the NH (blue) and SH (red) for three of the CMIT model simulations for three different seasons: June solstice 2003 ((first panel) jsol-mh), December solstice 2002 ((second panel) dsol-hh), and March equinox 2003 ((third panel) meq-mh), and the NH-SH differences between these simulations (fourth panel). All results are plotted against the day of year (DOY) for March equinox 2003 on the *x* axis, with the results for December solstice 2002 and June solstice 2003 shifted as indicated. The NH-SH differences were smoothed with a running boxcar average of 11 points to allow the different curves to be distinguished more clearly.

Table 2 and also shown graphically in Figure 3. Color codes in Figure 3 provide an indication of solar and geomagnetic activity levels. The simulations from Figure 2 (high solar and geomagnetic activity) are indicated in red. For these cases, we can compare all three seasons. The average ion drift speed for both hemispheres is largest in March equinox, which does not correspond with the observations. Differences between the solstices may show somewhat better correspondence. For the NH, the simulated ion drift speeds are similar for both solstices, while they are clearly higher at June solstice than December solstice in the SH. Examining Figure 1 again (for the high solar activity case), it does appear that these features are also present in the observations.

In terms of north-south asymmetries in ion drift speeds, the model reproduces the key features of the observations quite well. The NH ion drift speeds are almost always larger than in the SH, which we also find when

Table 2. High-Latitude Ion Drifts Speeds Averaged Over Each Simulation Interval for the NH and SH With 95% Confidence Intervals[a]

	Mean Ion Drift Speed (m/s)						
Identifier	NH			SH			NH-SH
dsol-hh	459.9	±	7.9	372.6	±	5.8	**87.3**
jsol-mh	463.6	±	6.3	452.3	±	6.8	11.4
meq-mh	595.7	±	10.8	507.2	±	9.3	**88.5**
dsol-mm	393.0	±	5.7	320.5	±	4.6	**72.5**
dsol-ll	312.1	±	4.0	274.3	±	3.2	**37.8**
jsol-lm	319.7	±	4.1	261.4	±	3.9	**58.3**
dsol-lh	470.6	±	8.3	420.8	±	6.6	**49.8**
jsol-lh	510.3	±	6.9	462.4	±	7.0	**47.9**

[a]The NH-SH differences are also shown and printed in bold when significant.

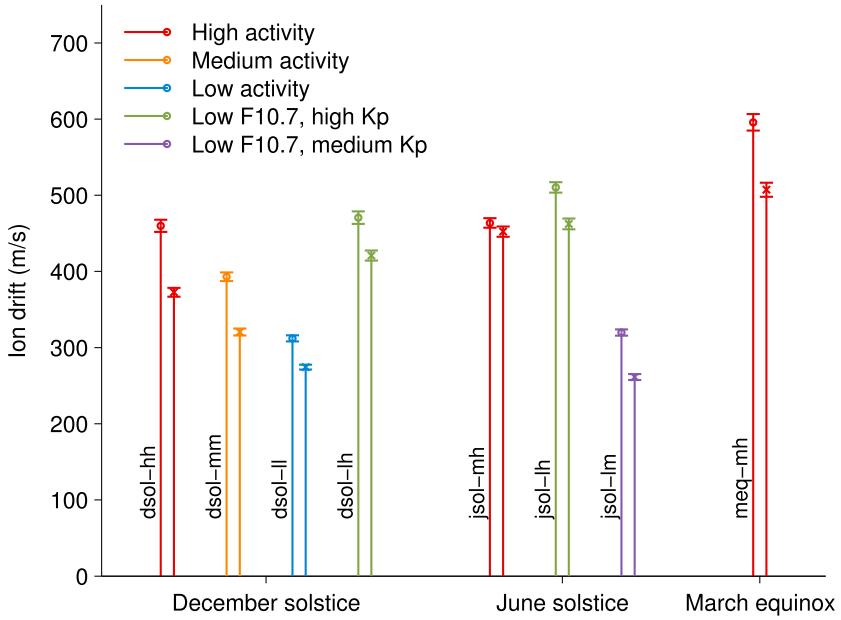

Figure 3. Mean ion drift speed in the polar cap (>80° magnetic latitude) shown in pairs for the NH (left) and SH (right) for each of the CMIT model simulations, time averaged over each simulation interval. The 95% confidence intervals are shown as error bars. Color codes provide an indication of the level of solar and geomagnetic activity: red-both high; orange-both medium; blue-both low; green-low solar (radiative) activity, but high geomagnetic activity; purple-low solar (radiative) activity, but medium geomagnetic activity.

including all observations from Cluster/EDI. The only exception to this is the high solar activity June solstice case (jsol-mh). The other simulations done for June solstice, with lower solar activity levels, do show a clear north-south asymmetry on the order of ~50 m/s. This again agrees very well with the observational results. Note that the only difference between the jsol-mh and jsol-lh simulations is the $F_{10.7}$ level (solar wind conditions are the same), proving that it is really the difference in solar radiative forcing that produces the difference in north-south asymmetry between these cases. For December solstice, a reduction in solar activity level reduces the north-south asymmetry in the simulations but does not remove the asymmetry completely, as seems to be the case in the observations. Differences in the average geomagnetic activity level do not appear to have a substantial effect on the north-south asymmetries.

We have demonstrated in previous work that the north-south asymmetry in ion drift speed during equinox is due to the asymmetry in the magnetic field [*Förster and Cnossen*, 2013], as explained in section 1. Now we will explain how the effects of magnetic field asymmetry interact with the seasonal cycle and solar activity level. The summer hemisphere always receives more sunlight than the winter hemisphere and therefore has higher conductivity. This affects the coupling between the magnetosphere and ionosphere. In the CMIT model this is described by the following equation:

$$\nabla_{\perp} \cdot (\Sigma \cdot \nabla_{\perp} \Phi) = J_{//} \tag{1}$$

where Φ is the electric field potential, Σ is the ionospheric conductance (the height-integrated conductivity), and $J_{//}$ is the upward field-aligned current. It follows from this that a higher ionospheric conductance, as occurs in summer, will lead to a weaker electric field and/or stronger field-aligned currents. In practice, a balance is reached through some adjustment in both variables, but we do find that the cross-polar cap potential (CPCP, normally a good measure of the strength of the electric field) is systematically lower in summer than in winter. Averages of the CPCP in the same format as for ion drift speeds are shown in Table 3 (see also similar results by *Cnossen et al.* [2012b]). The larger CPCP in winter acts to produce larger ion drift speeds in winter. During June solstice (SH winter) this seasonal (summer-winter) effect therefore favors larger ion drift speeds in the SH, opposing the effect of magnetic field asymmetry, while during December solstice (NH winter), both seasonal (summer-winter) and magnetic field effects favor larger ion drift speeds in the NH. This explains why we find a larger north-south asymmetry in ion drift speed for December solstice (two effects acting together)

Table 3. Cross-Polar Cap Potential (CPCP) Averaged Over Each Simulation Interval for the NH and SH With 95% Confidence Intervals[a]

	Mean CPCP (kV)						
Identifier	NH			SH			NH-SH
dsol-hh	62.4	±	1.2	55.4	±	1.0	**7.0**
jsol-mh	63.2	±	1.0	72.8	±	1.2	**−9.5**
meq-mh	83.6	±	1.7	85.0	±	1.7	−1.3
dsol-mm	52.5	±	0.9	47.1	±	0.8	**5.4**
dsol-ll	42.1	±	0.6	40.6	±	0.5	**1.5**
jsol-lm	39.7	±	0.6	41.0	±	0.6	**−1.3**
dsol-lh	64.5	±	1.2	61.7	±	1.1	**2.8**
jsol-lh	68.7	±	1.0	74.8	±	1.2	**−6.1**

[a]The NH-SH differences are also shown and printed in bold when significant.

than for June solstice (two effects partly canceling out) when solar activity is high. When solar activity is low, the seasonal (summer-winter) effect will be weaker, so that the north-south asymmetry gets weaker for December solstice and stronger for June solstice.

It may be a surprising result that we obtain a difference in CPCP between summer and winter. The CPCP is generally thought to be directly related to the magnetic reconnection process between the solar wind and magnetosphere, with the magnetospheric convection potential being mapped down to the polar ionosphere along equipotential geomagnetic field lines. This should lead to the same CPCP in both hemispheres. However, if one considers that the ionosphere can influence the magnetic reconnection process, rather than only respond to the forcing from the magnetosphere, it becomes conceivable that there could be small but systematic differences between summer and winter. *Papitashvili and Rich* [2002], for instance, offer further discussion on this possibility.

We do note that it is still unclear whether a summer-winter difference in CPCP exists in the real world; some studies have reported a larger CPCP in winter [*de la Beaujardière et al.*, 1991; *Papitashvili and Rich*, 2002; *Zhang et al.*, 2007], in agreement with what the model shows, but others have found a larger CPCP in summer [*Weimer*, 1995; *Ruohoniemi and Greenwald*, 2005; *Pettigrew et al.*, 2010]. It may be that measurements of the CPCP are simply not precise enough to be able to distinguish the relatively small (~10%) summer-winter differences. However, the good agreement between our observations and simulations in terms of the summer-winter variations of the north-south asymmetry in ion drift speed suggests that the model is behaving realistically.

4. Neutral Wind Speed

Figure 4 shows the average neutral wind speed in the polar cap (>80° magnetic latitude) based on CHAMP data as a function of day of year in both hemispheres. Even though ion drag is an important term in the high-latitude momentum budget of the thermosphere, the seasonal variation in neutral wind speed clearly behaves differently from the seasonal variation in ion drift speeds. While the high-latitude ion drift speeds showed a semiannual variation, the neutral wind speeds show an annual variation. Both high and low solar activity years show larger neutral wind speeds in the NH around June solstice and in the SH around December solstice, i.e., neutral winds are strongest in the summer hemisphere. The differences between summer and winter appear to be slightly larger around June solstice than December solstice. The transitions between maxima and minima in neutral wind speed tend to occur approximately a month after equinox. We are not sure what causes this delay, but perhaps this represents the time needed for the upper atmosphere to fully adjust to the changing solar illumination. On the other hand, it is also possible that the delay is not actually significant.

The simulation results for the high-latitude neutral wind speeds are summarized in Table 4 and Figure 5, following the format of Table 2 and Figure 3, respectively. CMIT does not reproduce the seasonal variations in neutral wind speed that were found in the observations very well. This points to a problem with the model which we will further discuss below. For the high solar activity cases, marked in red, the model shows

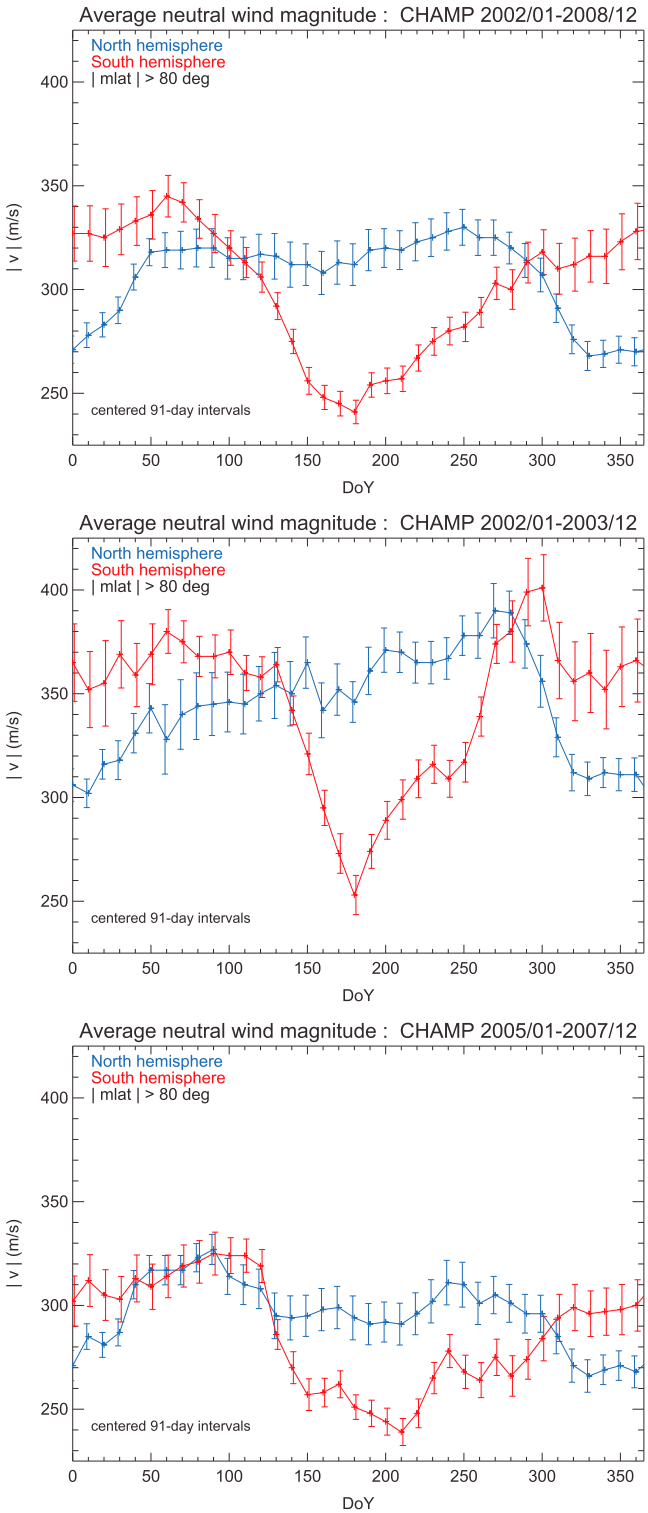

Figure 4. 91 day running averages of the mean neutral wind speed in the polar cap (>80° magnetic latitude) for the NH (blue) and SH (red) based on CHAMP data from (top) January 2002 to December 2008 and separately for high solar activity years ((middle) 2002–2003) and low solar activity years ((bottom) 2005–2007). Error bars represent the 95% confidence intervals on the means.

Table 4. High-Latitude Neutral Wind Speeds Averaged Over Each Simulation Interval for the NH and SH With 95% Confidence Intervals[a]

	Mean Neutral Wind Speed (m/s)						
Identifier	NH			SH			NH-SH
dsol-hh	359.0	±	5.5	326.5	±	4.0	**32.5**
jsol-mh	366.6	±	3.0	333.8	±	3.9	**32.7**
meq-mh	472.6	±	5.8	408.1	±	4.9	**64.5**
dsol-mm	291.2	±	3.3	270.6	±	2.6	**20.7**
dsol-ll	217.9	±	2.0	221.5	±	1.8	−3.7
jsol-lm	213.9	±	1.5	168.5	±	1.2	**45.4**
dsol-lh	278.8	±	3.9	274.7	±	3.1	4.0
jsol-lh	313.1	±	2.4	264.8	±	2.8	**48.3**

[a]The NH-SH differences are also shown and printed in bold when significant.

strongest neutral wind speeds in March equinox, instead of either of the solstices, and for nearly all cases the simulated neutral wind speeds are larger in the NH than in the SH, almost regardless of the season. The model results only start to resemble the observations somewhat more closely for low solar activity: in those cases there is no longer a significant north-south asymmetry during December solstice, while neutral winds are still stronger in the NH than the SH during June solstice, i.e., in the summer hemisphere. In general, however, the CMIT model appears to be biased toward too strong neutral winds in the NH.

The neutral wind speeds simulated by CMIT are quite similar to the simulated ion drift speeds. This is not necessarily unreasonable in the polar cap area, where neutral winds do tend to be closely coupled to the ion drifts. However, the seasonal variations in the simulated neutral wind speeds are also remarkably similar to the seasonal variations in the ion drifts speeds—much more so than is the case in the observations. This suggests that the ion-neutral coupling in the model may be too strong or does not follow the correct seasonal cycle. Above ~150 km it is mainly the Pedersen ion drag coefficient that describes this coupling, and this is roughly proportional to the electron density [*Richmond*, 1995]. Further investigation of the seasonal cycle in electron density produced by the CMIT model indeed revealed a problem with this. In principle, one would

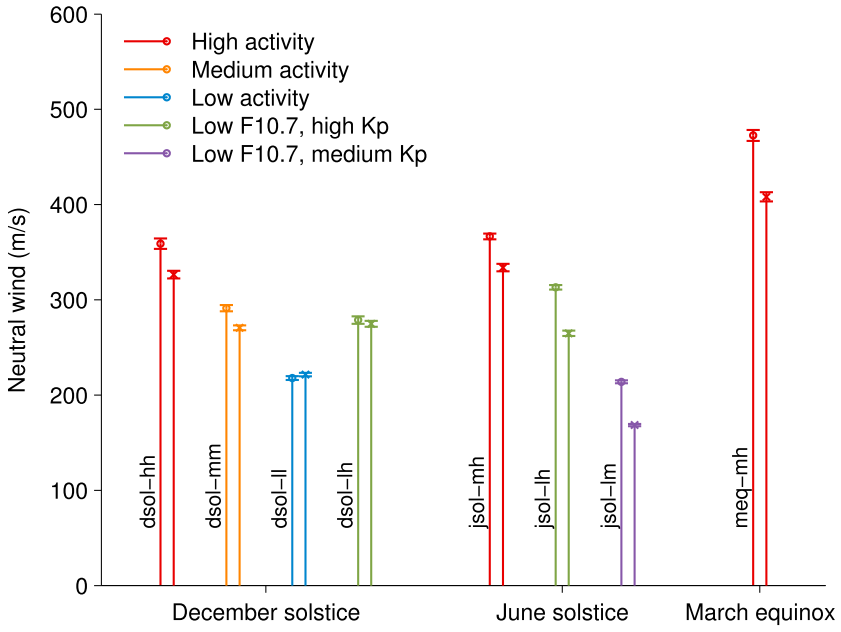

Figure 5. Mean neutral wind speed in the polar cap (>80° magnetic latitude) shown in pairs for the NH (left) and SH (right) for each of the CMIT model simulations, time-averaged over each simulation interval. The 95% confidence intervals are shown as error bars. Color codes provide an indication of the level of solar and geomagnetic activity: red-both high; orange-both medium; blue-both low; green-low solar (radiative) activity, but high geomagnetic activity; purple-low solar (radiative) activity, but medium geomagnetic activity.

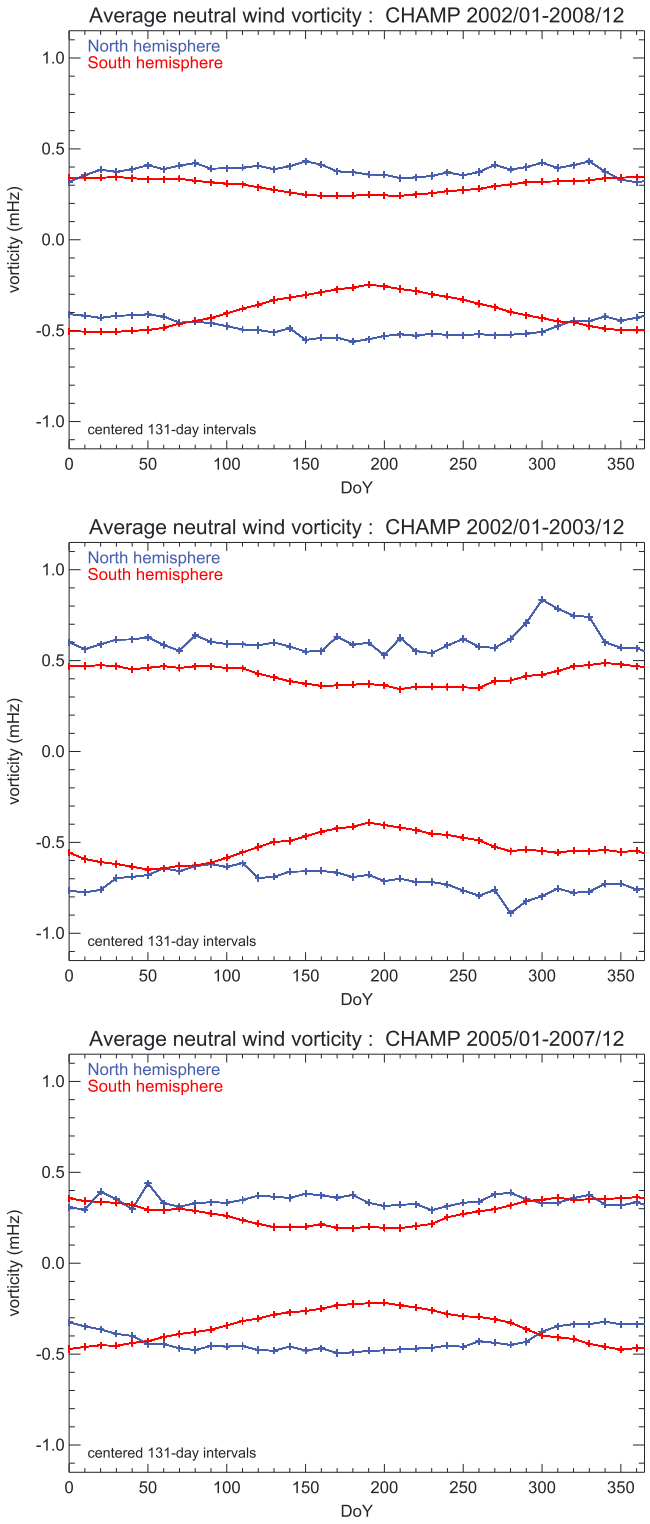

Figure 6. 131 day running averages of the maxima and minima of the high-latitude neutral wind vorticity in the NH (blue) and SH (red) based on CHAMP data from (top) January 2002 to December 2008 and separately for high solar activity years ((middle) 2002–2003) and low solar activity years ((bottom) 2005–2007). Maxima indicate the strength of the dawn cell; minima the strength of the dusk cell.

Table 5. Neutral Wind Vorticity Minima, Indicative of the Strength of the Duskside Vortex, Averaged Over Each Simulation Interval for the NH and SH With 95% Confidence Intervals[a]

	Neutral Wind Vorticity Minimum (MHz)						
Identifier	NH			SH			NH-SH
dsol-hh	−0.516	±	0.008	−0.360	±	0.005	**−0.156**
jsol-mh	−0.391	±	0.004	−0.386	±	0.005	−0.005
meq-mh	−0.510	±	0.007	−0.472	±	0.007	**−0.038**
dsol-mm	−0.391	±	0.005	−0.344	±	0.004	**−0.047**
dsol-ll	−0.237	±	0.003	−0.218	±	0.002	**−0.019**
jsol-lm	−0.211	±	0.002	−0.136	±	0.002	**−0.075**
dsol-lh	−0.365	±	0.006	−0.267	±	0.003	**−0.098**
jsol-lh	−0.307	±	0.003	−0.264	±	0.003	**−0.043**

[a]The NH-SH differences are also shown and printed in bold when significant.

expect larger electron densities in the summer hemisphere than in the winter hemisphere due to more ionization from solar radiation in summer. Observations of the electron density at 400 km made by CHAMP confirm this picture [*Liu et al.*, 2007]. However, the CMIT model tends to predict slightly larger electron densities around 400 km in the winter polar region. This appears to be associated primarily with an incorrect vertical distribution of plasma in the model. Both the height of the peak electron density and the peak electron density itself tend to be higher in winter than in summer at high latitudes, in disagreement with observations made by the Constellation Observing System for Meteorology, Ionosphere, and Climate (COSMIC) program (N. Pedatella, personal communication, 2015), while the modeled total electron content (TEC) is larger in the summer hemisphere, as expected, and in agreement with COSMIC observations. *Qian et al.* [2013] found similar discrepancies in the high-latitude peak electron density and its height between COSMIC observations and the TIE-GCM (the upper atmosphere component of CMIT). The incorrect seasonal cycle in electron density around 400 km will introduce errors in the ion drag force acting on the neutral wind, making it too strong in winter and too weak in summer. This could help explain the discrepancies between the observed and simulated seasonal variations of the neutral wind and their north-south asymmetry. Why the model does not correctly capture the observed seasonal variation in the vertical plasma distribution is not clear yet and needs to be further investigated in future work.

We do note that there are also errors associated with the CHAMP observations of the neutral wind. These are mainly due to errors in the calibration of the accelerometer and errors in the external model used to retrieve the neutral winds. We minimize these through the iterative method developed by *Doornbos et al.* [2010] and assume that they mostly average out by the statistical approach we take. However, the errors do depend on the orbit geometry, which could potentially affect the observed north-south asymmetry. In addition, the aerodynamic accelerations from which the wind speeds are derived will be smaller when the neutral density is low, as in winter or for low solar activity, resulting in relatively larger errors under those conditions. This could also introduce biases in the seasonal variations we observe with CHAMP. Still, we do not expect these biases to be so large that they could explain the discrepancy between the observed and simulated variations in the neutral winds.

5. Neutral Wind Vorticity

Figure 6 shows the seasonal variation of the observed maximum and minimum values of the neutral wind vorticity. The same simulation results are also summarized in Tables 5 and 6. The maxima indicate the strength of the dawn cell and the minima the strength of the dusk cell (see *Förster et al.* [2011] for an example of the full vorticity pattern and the corresponding neutral wind vector pattern at 400 km altitude for 2002–2003). In terms of seasonal variation, the maxima and minima of the neutral wind vorticity behave differently from the neutral wind speed and clearly more similarly to the ion drift speeds. The absolute vorticity values are on average larger in the NH, but this is more pronounced around June solstice. Around December solstice, the north-south asymmetry disappears or even reverses, but not as dramatically as was the case for the neutral wind speeds. The low solar activity years show very similar behavior as the full data set. The high solar activity years show a larger absolute vorticity in the NH in general, with less systematic seasonal dependence.

Table 6. Neutral Wind Vorticity Maxima, Indicative of the Strength of the Dawnside Vortex, Averaged Over Each Simulation Interval for the NH and SH With 95% Confidence Intervals[a]

	Neutral Wind Vorticity Maximum (MHz)						
Identifier	NH			SH			NH-SH
dsol-hh	0.483	±	0.008	0.347	±	0.005	**0.136**
jsol-mh	0.305	±	0.003	0.400	±	0.005	**−0.095**
meq-mh	0.372	±	0.005	0.358	±	0.004	**0.014**
dsol-mm	0.410	±	0.005	0.260	±	0.002	**0.150**
dsol-ll	0.276	±	0.003	0.210	±	0.002	**0.066**
jsol-lm	0.172	±	0.002	0.197	±	0.002	**−0.025**
dsol-lh	0.334	±	0.005	0.251	±	0.003	**0.083**
jsol-lh	0.238	±	0.002	0.316	±	0.003	**−0.078**

[a]The NH-SH differences are also shown and printed in bold when significant.

We further note that the seasonal cycle in absolute vorticity is noticeably larger in the SH than in the NH. This is primarily responsible for the seasonal variations in north-south asymmetry.

The model results for the vorticity maxima and minima are shown in Figure 7. The dusk cell, represented by the vorticity minima (absolute values are plotted), is significantly stronger in the NH than the SH for almost all cases. Only the high activity case for June solstice (jsol-mh) shows no significant north-south asymmetry. In contrast, for the December solstice cases the asymmetry seems stronger for the higher activity cases, although this is perhaps more related to geomagnetic activity rather than solar (radiative) activity (compare dsol-ll in blue with dsol-lh in green). The modeled seasonal variation in north-south asymmetry does not match with the observations, although the generally larger absolute vorticity in the NH does match. The dawn cell, represented by the vorticity maxima, is also stronger in the NH than the SH for December solstice, but for June solstice the asymmetry is reversed. This seasonal variation is opposite to what the observations are showing.

The poor agreement between the observed and simulated seasonal variation in the strength of the neutral wind vortices is probably related again to an incorrect seasonal cycle in plasma density around 400 km in CMIT, as discussed in section 4. A too weak ion drag force in summer and too strong ion drag force in winter will make the NH neutral wind vortices too weak and SH neutral wind vortices too strong in June solstice. The opposite will be the case in December solstice. Our model simulations are therefore likely to be overestimating the north-south asymmetry for December solstice and getting it the wrong way around for June solstice. Once again, this is an issue with the CMIT model that needs to be addressed in future work.

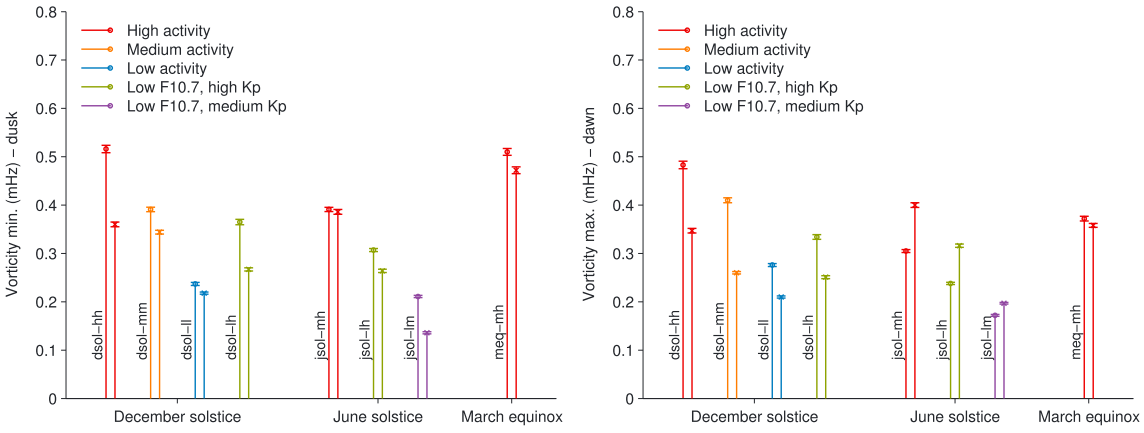

Figure 7. Absolute values of the maxima (right) and minima (left) of the high-latitude neutral wind vorticity shown in pairs for the NH (left) and SH (right) for each of the CMIT model simulations, time averaged over each simulation interval. The 95% confidence intervals are shown as error bars. Maxima indicate the strength of the dawn cell; minima the strength of the dusk cell. Color codes provide an indication of the level of solar and geomagnetic activity: red-both high; orange-both medium; blue-both low; green-low solar (radiative) activity, but high geomagnetic activity; purple-low solar (radiative) activity, but medium geomagnetic activity.

6. Summary and Concluding Remarks

Observations of ion drifts and neutral winds over almost a full solar cycle have been analyzed to show for the first time how asymmetries between the NH and SH polar upper atmosphere vary with season and solar/geomagnetic activity. On average, ion drift speeds in the polar cap (>80° magnetic latitude) are larger in the NH than in the SH, with little dependence on season when all available data are used (2001–2013). However, for solar maximum years (2002–2003) the asymmetry disappears around June solstice, while this happens around December solstice for solar minimum years (2005–2007). The high-latitude neutral wind vortices at dawn and dusk, which represent the part of the neutral wind field that is most directly related to the ion drifts, show similar behavior; they tend to be stronger in the NH, except around December solstice, in particular, when solar activity is low. In contrast, the neutral wind speeds in the polar cap are always larger in the summer hemisphere, regardless of the phase of the solar cycle.

Based on comparisons with simulations with the CMIT model, the following picture has emerged to explain several key features of the observational results. The high-latitude electric field in the two hemispheres is more or less equal under equinox conditions, but at solstice it is stronger in the winter hemisphere, due to the lower ionospheric conductivity there. This is at least what the model suggests. Summer-winter differences are stronger for higher solar activity.

The summer-winter difference in the electric field directly affects the high-latitude ion drift speeds, with a stronger electric field favoring larger ion drifts. However, the ion drifts are also influenced by asymmetry in the Earth's magnetic field. The weaker magnetic field strength at NH high latitudes acts to produce larger ion drifts in the NH than the SH, regardless of the season. During June solstice this magnetic field effect opposes the seasonal summer-winter effect. When solar activity is high, the summer-winter effect is strong and mostly balances the magnetic field effect, so that there is little asymmetry in ion drift speeds during that time of year. For low solar activity, the summer-winter effect is weaker and does not completely counteract the magnetic field effect, so that the ion drift speeds are larger in the NH than in the SH for June solstice. It is not clear why the observations show no significant asymmetry around December solstice when solar activity is low. This is one feature that needs to be checked with other observations, and if these confirm our finding, further work is needed to explain it.

The high-latitude neutral winds are affected by the ion drifts through the ion drag force. This force should be stronger in summer than in winter due to larger electron density in summer [see also *Kwak and Richmond*, 2007]. Unfortunately, the CMIT model does not appear to be describing the seasonal variation in the ion drag force correctly, as the high-latitude electron density in CMIT at ~400 km is slightly larger in winter than in summer (for as yet unknown reasons). We suspect that this is the reason that the simulated seasonal variation in neutral winds does not match the observations. On the other hand, we do not think that this problem has serious implications for our simulated ion drift speeds, as these are primarily driven by forcing from the magnetosphere. Effects of errors in electron density and neutral winds on ion drift speeds should therefore be small. The relatively good agreement between the observations and model results in terms of ion drift speeds supports that. Still, the incorrect seasonal cycle in TEC is clearly an issue that needs to be addressed in the CMIT model. Our observational results provide a clear benchmark for the model to aim for.

While the problem with the ion drag force in CMIT is a significant one, there are also other factors that could play a role in north-south asymmetries in neutral winds. For instance, we have not included possible influences from north-south differences in the lower atmosphere, other than those imposed by the tidal forcing at the lower boundary of the CMIT model (at ~97 km). We do not know whether this is an important factor or not. It would require a study in its own right to determine this, because it is not only dependent on the magnitude and structure of north-south asymmetries at the lower boundary but also on whether such asymmetries are associated with tidal components that are important in the high-latitude upper thermosphere. *Becker et al.* [2015] recently showed that differences in the temperature and dynamics in the troposphere and stratosphere have significant effects on the polar mesosphere. There is also evidence for influences of forcing from below at higher altitudes, but primarily for the middle- to low-latitude ionosphere and thermosphere, where tidal amplitudes are larger [e.g., *Goncharenko et al.*, 2010]. Still, systematic differences in lower boundary forcing between the NH and SH could potentially affect the thermosphere dynamics at higher latitudes as well. To investigate this, modeling with a whole atmosphere model will be needed. In addition, more advanced analyses of north-south differences will benefit from additional observations to verify the

results obtained with CHAMP and Cluster/EDI. Such activities are indeed planned through a new collaborative project, organized through an International Space Science Institute team. This will combine measurements from various sources (other satellites and ground-based Fabry-Pérot Interferometers) to verify the observational results presented here and will use additional models to explain them.

Acknowledgments

This study is part of the British Antarctic Survey Polar Science for Planet Earth Programme. Ingrid Cnossen was funded by Natural Environment Research Council (NERC) fellowship NE/J018058/1. We acknowledge the International Space Science Institute for support for our international team on "Magnetosphere-Ionosphere-Thermosphere Coupling: Differences and similarities between the two hemispheres". The CMIT simulations were performed on the Yellowstone high-performance computing facility (ark:/85065/d7wd3xhc) provided by the Computational and Information Systems Laboratory of the National Centre for Atmospheric Research, sponsored by the National Science Foundation. We thank Nick Pedatella for providing us with plots of COSMIC electron density data for comparison with CMIT results. CHAMP data can be obtained from the Information System and Data Center for geoscientific data hosted by GFZ Potsdam at: http://isdc.gfz-potsdam.de/index.php. The CHAMP mission was sponsored by the Space Agency of the German Aerospace Center (DLR) through funds of the Federal Ministry of Economics and Technology, following a decision of the German Federal Parliament (grant code 50EE0944). Cluster data can be obtained from the Cluster Active Archive hosted by the European Space Agency at: http://caa.estec.esa.int/caa/. Modeling results will be published as a separate data set under doi:10/8bm. I. Cnossen can be contacted for further information on these data or for additional modeling results.

References

Baker, K. B., and S. Wing (1989), A new magnetic coordinate system for conjugate studies at high latitudes, *J. Geophys. Res.*, *94*, 9139–9143.

Becker, E., R. Knöpfel, and F.-J. Lübken (2015), Dynamically induced hemispheric differences in the seasonal cycle of the summer polar mesopause, *J. Atmos. Sol. Terr. Phys.*, *129*, 128–141.

Cnossen, I., and A. D. Richmond (2012), How changes in the tilt angle of the geomagnetic dipole affect the coupled magnetosphere-ionosphere-thermosphere system, *J. Geophys. Res.*, *117*, A10317, doi:10.1029/2012JA018056.

Cnossen, I., A. D. Richmond, M. Wiltberger, W. Wang, and P. Schmitt (2011), The response of the coupled magnetosphere-ionosphere-thermosphere system to a 25% reduction in the dipole moment of the Earth's magnetic field, *J. Geophys. Res.*, *116*, A12304, doi:10.1029/2011JA017063.

Cnossen, I., A. D. Richmond, and M. Wiltberger (2012a), The dependence of the coupled magnetosphere-ionosphere-thermosphere system on the Earth's magnetic dipole moment, *J. Geophys. Res.*, *117*, A05302, doi:10.1029/2012JA017555.

Cnossen, I., M. Wiltberger, and J. E. Ouellette (2012b), The effects of seasonal and diurnal variations in the Earth's magnetic dipole orientation on solar wind-magnetosphere-ionosphere coupling, *J. Geophys. Res.*, *117*, A11211, doi:10.1029/2012JA017825.

de la Beaujardière, O., D. Alcayde, J. Fontanari, and C. Leger (1991), Seasonal dependence of high-latitude electric fields, *J. Geophys. Res.*, *96*(A4), 5723–5735, doi:10.1029/90JA01987.

Doornbos, E., J. van den IJssel, H. Lühr, M. Förster, and G. Koppenwallner (2010), Neutral density and crosswind determination from arbitrarily oriented multiaxis accelerometers on satellites, *J. Spacecr. Rockets*, *47*, 580–589.

Escoubet, C. P., R. Schmidt, and M. L. Goldstein (1997), Cluster—Science and mission overview, *Space Sci. Rev.*, *79*, 11–32.

Förster, M., and I. Cnossen (2013), Upper atmosphere differences between northern and southern high latitudes: The role of magnetic field asymmetry, *J. Geophys. Res. Space Physics*, *118*, 5951–5966, doi:10.1002/jgra.50554.

Förster, M., and S. Haaland (2015), Interhemispheric differences in ionospheric convection: Cluster EDI observations revisited, *J. Geophys. Res. Space Physics*, *120*, 5805–5823, doi:10.1002/2014JA020774.

Förster, M., G. Paschmann, S. E. Haaland, J. M. Quinn, R. B. Torbert, H. Vaith, and C. A. Kletzing (2007), High-latitude plasma convection from Cluster EDI: Variances and solar wind correlations, *Ann. Geophys.*, *25*, 1691–1707.

Förster, M., S. Rentz, W. Köhler, H. Liu, and S. E. Haaland (2008), IMF dependence of high-latitude thermospheric wind pattern derived from CHAMP cross-track measurements, *Ann. Geophys.*, *26*, 1581–1595.

Förster, M., S. E. Haaland, and E. Doornbos (2011), Thermospheric vorticity at high geomagnetic latitudes from CHAMP data and its IMF dependence, *Ann. Geophys.*, *29*(1), 181–186.

Goncharenko, L. P., J. L. Chau, H.-L. Liu, and A. J. Coster (2010), Unexpected connections between the stratosphere and ionosphere, *Geophys. Res. Lett.*, *37*, L10101, doi:10.1029/2010GL043125.

Haaland, S. E., G. Paschmann, M. Förster, J. M. Quinn, R. B. Torbert, C. E. McIlwain, H. Vaith, P. A. Puhl-Quinn, and C. A. Kletzing (2007), High-latitude plasma convection from Cluster EDI measurements: Method and IMF-dependence, *Ann. Geophys.*, *25*(1), 239–253.

Hagan, M. E., and J. M. Forbes (2002), Migrating and non-migrating diurnal tides in the middle and upper atmosphere excited by tropospheric latent heat release, *J. Geophys. Res.*, *107*(D24), 4754, doi:10.1029/2001JD001236.

Hagan, M. E., and J. M. Forbes (2003), Migrating and non-migrating semidiurnal tides in the middle and upper atmosphere excited by tropospheric latent heat release, *J. Geophys. Res.*, *108*(A2), 1062, doi:10.1029/2002JA009466.

Kwak, Y.-S., and A. D. Richmond (2007), An analysis of the momentum forcing in the high-latitude lower thermosphere, *J. Geophys. Res.*, *112*, A01306, doi:10.1029/2006JA011910.

Liu, H., C. Stolle, S. Watanabe, T. Abe, M. Rother, and D. L. Cooke (2007), Evaluation of the IRI model using CHAMP observations in polar and equatorial regions, *Adv. Space Res.*, *39*, 904–909.

Lyon, J. G., J. A. Fedder, and C. M. Mobarry (2004), The Lyon-Fedder-Mobarry (LFM) global MHD magnetospheric simulation code, *J. Atmos. Sol. Terr. Phys.*, *66*(15–16), 1333–1350, doi:10.1016/j.jastp.2004.04.020.

Merkin, V. G., and J. G. Lyon (2010), Effects of the low-latitude ionospheric boundary condition on the global magnetosphere, *J. Geophys. Res.*, *115*, A10202, doi:10.1029/2010JA015461.

Papitashvili, V. O., and F. J. Rich (2002), High-latitude ionospheric convection models derived from Defense Meteorological Satellite Program ion drift observations and parameterized by the interplanetary magnetic field strength and direction, *J. Geophys. Res.*, *107*(A8), 1198, doi:10.1029/2001JA000264.

Pettigrew, E. D., S. G. Shepherd, and J. M. Ruohoniemi (2010), Climatological patterns of high-latitude convection in the Northern and Southern Hemispheres: Dipole tilt dependencies and interhemispheric comparisons, *J. Geophys. Res.*, *115*, A07305, doi:10.1029/2009JA014956.

Qian, L., A. G. Burns, S. C. Solomon, and W. Wang (2013), Annual/semiannual variation of the ionosphere, *Geophys. Res. Lett.*, *40*, 1928–1933, doi:10.1002/grl.50448.

Reigber, C., H. Lühr, and P. Schwintzer (2002), CHAMP mission status, *Adv. Space Res.*, *30*, 129–134.

Richmond, A. D. (1995), Ionospheric electrodynamics, in *Handbook of Ionospheric Electrodynamics*, vol. II, pp. 249–290, CRC Press, Boca Raton, Fla.

Richmond, A. D., E. C. Ridley, and R. G. Roble (1992), A thermosphere/ionosphere general circulation model with coupled electrodynamics, *Geophys. Res. Lett.*, *19*(6), 601–604.

Roble, R. G., E. C. Ridley, A. D. Richmond, and R. E. Dickinson (1988), A coupled thermosphere/ionosphere general circulation model, *Geophys. Res. Lett.*, *15*, 1325–1328.

Ruohoniemi, J. M., and R. A. Greenwald (2005), Dependencies of high-latitude plasma convection: Consideration of interplanetary magnetic field, seasonal, and universal time factors in statistical patterns, *J. Geophys. Res.*, *110*, A09204, doi:10.1029/2004JA010815.

Tsyganenko, N. A. (2002a), A model of the near magnetosphere with a dawn-dusk asymmetry 1. Mathematical structure, *J. Geophys. Res.*, *107*(A8), 1179, doi:10.1029/2001JA000219.

Tsyganenko, N. A. (2002b), A model of the near magnetosphere with a dawn-dusk asymmetry 2. Parameterization and fitting to observations, *J. Geophys. Res.*, *107*(A8), 1176, doi:10.1029/2001JA000220.

Wang, W., M. Wiltberger, A. G. Burns, S. C. Solomon, T. L. Killeen, N. Maruyama, and J. G. Lyon (2004), Initial results from the coupled magnetosphere-ionosphere-thermosphere model: Thermosphere-ionosphere responses, *J. Atmos. Sol. Terr. Phys.*, *66*(15–16), 1425–1441, doi:10.1016/j.jastp.2004.04.008.

Wang, W., J. Lei, A. G. Burns, M. Wiltberger, A. D. Richmond, S. C. Solomon, T. L. Killeen, E. R. Talaat, and D. N. Anderson (2008), Ionospheric electric field variations during a geomagnetic storm simulated by a Coupled Magnetosphere Ionosphere Thermosphere (CMIT) model, *Geophys. Res. Lett.*, *35*, L18105, doi:10.1029/2008GL035155.

Weimer, D. R. (1995), Models of high-latitude electric potentials derived with a least error fit of spherical harmonic coefficients, *J. Geophys. Res.*, *100*(A10), 19,595–19,607, doi:10.1029/95JA01755.

Wiltberger, M., W. Wang, A. G. Burns, S. C. Solomon, J. G. Lyon, and C. C. Goodrich (2004), Initial results from the Coupled Magnetosphere-Ionosphere-Thermosphere model: Magnetospheric and ionospheric responses, *J. Atmos. Sol. Terr. Phys.*, *66*(15–16), 1411–1423, doi:10.1016/j.jastp.2004.04.026.

Wiltberger, M., R. S. Weigel, W. Lotko, and J. A. Fedder (2009), Modeling seasonal variations of auroral particle precipitation in a global-scale magnetosphere-ionosphere simulation, *J. Geophys. Res.*, *114*, A01204, doi:10.1029/2008JA013108.

Zhang, S.-R., J. M. Holt, and M. McCready (2007), High latitude convection based on long-term incoherent scatter radar observations in North America, *J. Atmos. Sol. Terr. Phys.*, *69*, 1273–1291, doi:10.1016/j.jastp.2006.08.017.